

# Elasticity and onset of frictional dissipation at a non-sliding multicontact interface

By L. Bureau, C. Caroli and T. Baumberger

Groupe de Physique des Solides, 2 place Jussieu, 75251 Paris cedex 05, France

We measure the elastic and dissipative responses of a multicontact interface, formed between the rough surfaces of two contacting macroscopic solids, submitted to a biased oscillating shear force. We evidence that beyond a linear viscoelastic regime, observed at low shear amplitude, the interface response exhibits a dissipative component which corresponds to the onset of frictional dissipation. The latter regime exists whereas the tangential force applied, far from the nominal static threshold, does not provoke any sliding. This result, akin to that of Mindlin for a single contact, leads us to extend his model of microslip to the case of an interface composed of multiple microcontacts. While describing satisfactorily the elastic response, the model fails to account quantitatively for the observed energy dissipation, which, we believe, results from the fact that the key assumption of local Coulomb friction in Mindlin's model is not legitimate at the sub-micrometer scale of the microslip zones within microcontacts between surface asperities.

Keywords: contact stress, frictional dissipation, Hertz-Mindlin contacts

## 1. Introduction

The frictional response of the contact between two macroscopic solids submitted to a shear force is commonly described, in the framework of Amontons-Coulomb's law, in terms of: (i) a static force threshold,  $F_s$ , below which no relative displacement is supposed to occur, and (ii) a dynamic friction coefficient defined when stationary sliding is established.

However, it is known that frictional dissipation in mechanical contacts starts to build up for shear forces lower than the nominal static threshold. This behaviour, which is important in mechanical engineering, for instance in problems of fretting or damping in structural joints (see e.g. Goodman 1959, Olsson 1995), also presents a fundamental interest related to the understanding of the microscopic mechanisms responsible for macroscopic friction. This issue was first extensively studied by Mindlin et al. (1951), Johnson (1955), Courtney-Pratt & Eisner (1956) and Goodman & Brown (1962), who evidenced that the displacement response of Hertzian macroscopic contacts submitted to an oscillating tangential force of amplitude  $F < F_s$  exhibited a hysteresis loop attributable to an interfacial dissipative process. In order to account for this energy loss, Mindlin et al. (1951) proposed

Y Corresponding author. e-mail: lionelbureau@college-de-france.fr. Present address: LPMC, College de France, 11 place Marcelin Berthelot, 75231 Paris cedex 05.

a model of ‘microslip’ within the contact zone, based on the following description (Cattaneo 1938): wherever in the contact zone the tangential ( $\tau$ ) and normal ( $\sigma$ ) local stresses obey  $\tau < \mu \sigma$  (with  $\mu$  the friction coefficient) no relative tangential displacement occurs. Otherwise, shear provokes slip so that, in the corresponding region, the stresses satisfy locally a Coulomb friction law:  $\tau = \mu \sigma$ . It is then predicted that the sheared contact is composed of a circular non-sliding zone surrounded by an annular slipping region whose width increases with the applied shear force.

Still, Mindlin’s description of incipient sliding raises a question: down to which length scale is such an assumption of local friction valid? Indeed, macroscopic solids generally exhibit rough surfaces which, when brought into contact, form a multi-contact interface (MCI), i.e. an interface composed of a dilute set of microcontacts between asperities. When addressing the problem of friction at such an interface, one may therefore wonder whether the use of a local friction law is legitimate when dealing with the micro-meter-sized contacts between surface asperities. This in turn raises the question of the spatial scale of the elementary dissipative events responsible for solid friction, a cutoff length below which a local friction law cannot be meaningful.

Recently, experiments performed on such MCIs showed that (Berthoud & Baumberger 1998):

for tangential forces  $F < F_s$ , the pinned interface responds elastically, via the reversible deformation of the load-bearing asperities. In this regime, the shear stiffness of the interface can be measured and is well accounted for within the framework of Greenwood’s model of contact between rough surfaces (Greenwood & Williamson 1966).

for  $F > F_s$ , a creeplike irreversible sliding of the solids occurs.

A detailed study of this regime of incipient sliding, below the nominal static threshold, should therefore provide information about the physical processes underlying frictional dissipation. In order to achieve the force control and the displacement resolution required to perform such a study, we have developed an experimental setup which allows to probe the response of a multicontact interface to a biased oscillating shear force, of amplitude  $F_{ac}$  about a finite mean value  $F_{dc}$ , while the maximum force applied  $F_{dc} + F_{ac} = F_{max}$ .  $F_s$  (Baumberger et al. 1998). We thus showed that the displacement response of a macroscopic slider submitted to such a harmonic tangential force exhibited three different regimes, depending on the amplitude  $F_{ac}$  (Bureau et al. 2001). These are illustrated on figure 1, which shows the response to a shear force modulation of slowly increasing amplitude: in region (i), at small  $F_{ac}$ , the center of mass of the slider oscillates about a constant average position, which means that no irreversible sliding occurs; in region (ii), corresponding to higher shear amplitudes, the slider enters a creeplike regime where the slipped distance increases continuously, up to a final regime of abruptly accelerating motion (region (iii)).

In the present article, we report an experimental study which focuses on the first regime of small shear amplitudes, in which the interface is pinned, i.e. oscillates about a fixed position. In section 2, we briefly present the principle of operation of the experimental setup. By measuring the in-phase and out-of-phase components of the displacement response of a MCI submitted to a harmonic shear force, we can

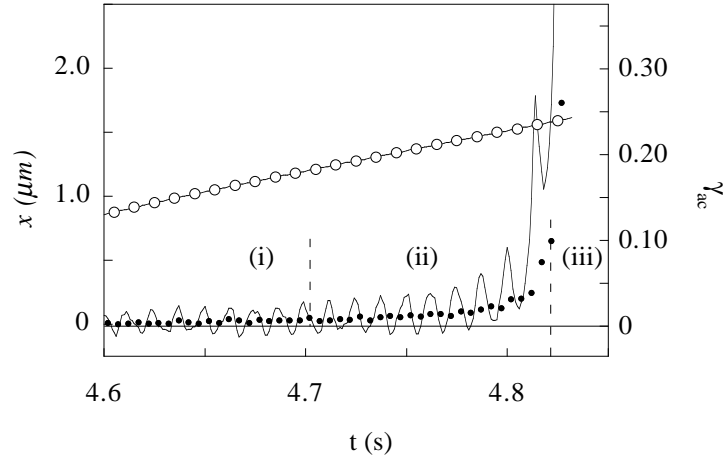


Figure 1. Time-plot of the instantaneous (line) and averaged ( ) displacement response of the slider to a biased oscillating shear force of increasing amplitude. On the right scale is plotted the reduced shear amplitude ( )  $\gamma_{ac}(t) = F_{ac}(t)/W$ , where  $W$  is the normal load. The bias used for this experiment is  $d_c = F_{dc}/W = 0.36$  and the frequency of oscillation  $f = 80$  Hz.

probe accurately both the elastic and dissipative responses of the interface (section 3). We evidence that:

the shear stress evolves with the ‘age’ of the interface, i.e. with the time elapsed since the solids were brought into contact, in agreement with the creep ageing of the load-bearing asperities already identified for such MCIs, which results in the slow logarithmic increase of microcontact radii (Dietrich & Kilgore 1994, Berthoud et al. 1999a),

frictional dissipation appears at shear forces well below the nominal static threshold, while no gross sliding is detected yet.

This latter point leads us to propose an extension of Mindlin’s model to the case of a multicontact interface, within the framework of Greenwood’s description for the contact of rough surfaces. We find that such a model of microslip within the contacts between asperities largely overestimates the energy dissipation, which we believe points out that a local description of friction is no longer valid at the sub-micrometric scale of the slip zones within the microcontacts forming multicontact interfaces.

## 2. Experiments

### (a) Samples

The multicontact interface studied here is formed between a slider and a track of commercial grade poly(methyl methacrylate) (PMMA). PMMA is a glassy polymer at room temperature ( $T_g \approx 120$  °C), of dynamic shear modulus  $G^0 = 2$  GPa and loss angle such that  $\tan \delta = 0.1$  at 100 Hz (Ferry 1980), and of quasi-static Young

modulus  $E' = 3 \text{ GPa}$ , Poisson ratio  $\nu = 0.44$  and hardness  $H' = 300 \text{ MPa}$  (Berthoud et al. 1999b).

The nominally flat surfaces of the slider ( $20 \times 20 \text{ mm}^2$ ) and of the track ( $25 \times 30 \text{ mm}^2$ ) are lapped with an abrasive aqueous suspension of SiC powder (mean particle size  $23 \text{ }\mu\text{m}$ ). This leads to a rms roughness of the samples  $R_q = 1.3 \text{ }\mu\text{m}$ , as previously characterized (Berthoud & Baumberger 1998).

Using Greenwood's result (Greenwood & Williamson 1966), assuming that: (i) the summit heights of asperities follow an exponential distribution of widths  $s = 1.3 \text{ }\mu\text{m}$ , and (ii) their mean radius of curvature  $\rho = 20 \text{ }\mu\text{m}$  (taken, as a conservative value, of the order of magnitude of the abrasive particle size), one can estimate, under the normal load  $W' = 2 \text{ N}$ , the number  $N$  of microcontacts:  $N' = \frac{W}{\rho s E s} \approx 100$  (where  $E = E'/(1 - \nu^2)$ ), and their mean radius  $a' = \sqrt{\frac{\rho W}{s E s}} \approx 5 \text{ }\mu\text{m}$ .

#### (b) Experimental setup: an inertial tribometer

The experimental setup, extensively described elsewhere (Baumberger et al. 1998) is based on the following principle. The track, on which the slider sits under its own weight  $mg$ , is first inclined at a given angle such that the ratio of the tangential ( $F_{dc}$ ) to normal ( $W$ ) load  $F_{dc}/W = \tan \theta_s$ . A harmonic motion, of controlled amplitude and frequency, is then imposed to the track, which results in an inertial oscillating shear force acting on the center of mass of the slider (see figure 2). In order to avoid torques and tilt motion, the slider sample is clamped in a metal part specially designed such that the center of mass of the slider is located in the plane of the interface.

The harmonic shear force on the interface thus reads, in the low frequency limit where the slider responds quasi-statically (see Baumberger et al. 1998),  $F(t) = F_{ac} \cos(\omega t)$  with  $F_{ac} = m a$ , where  $a$  is the imposed acceleration amplitude of the track. We denote  $\alpha_{dc} = F_{dc}/W$  and  $\alpha_{ac} = F_{ac}/W$ . These control parameters can be set in the ranges  $0 < \alpha_{dc} < 0.58$  and  $0 < \alpha_{ac} < 0.6$ . The frequency of the oscillating tangential force can be chosen between 15 and 100 Hz, this upper limit ensuring the quasi-static condition for the slider motion.

We measure, in response to this excitation, the displacement  $x(t)$  of the slider relatively to the track, by means of a capacitive gauge. Its signal is sent to a lock-in amplifier, which allows to detect, within  $1 \text{ nm}$ , the in-phase ( $x_0$ ) and out-of-phase ( $x_{90}$ ) components of the displacement with respect to the harmonic input. We thus have access to the elastic and dissipative responses of the multicontact interface.

#### (c) Reproducibility

The scattering of the results thus obtained depends crucially on the way the interface is prepared. We have tested two different protocols:

1. This estimation assumes that contacting asperities are deformed elastically. Actually, Greenwood's plasticity index  $\psi = (E/H) \sqrt{s} \approx 2.5$  for our surfaces, which indicates that most contacting asperities have started to yield plastically. However, since  $\psi$  is still of order unity, the set of asperities is in fact in an elastic-plastic state of deformation (Berthoud et al. 1999b), far from the fully plastic limit. We therefore use, for our rough estimate of  $N$ , the expression corresponding to the elastic limit (evaluating  $N$  in the fully plastic limit would lead to a number of microcontacts times larger).

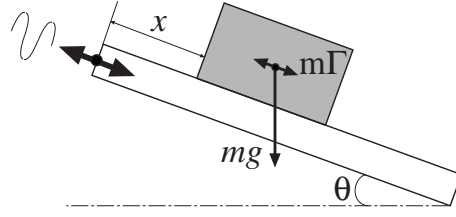


Figure 2. Principle of operation of the inertial tribometer: the slider on the inclined track is submitted to a constant tangential force  $F_{dc} = mg \sin \theta$  on which is superimposed a harmonic shear force of amplitude  $m\Gamma$ , where  $\Gamma$  is the imposed acceleration amplitude of the track. We measure the displacement  $x$  of the slider with respect to the track.

(i) after the slider is put into contact with the inclined track, a time  $t_w$  is waited during which the interface is left under constant normal and tangential loads. At the end of this waiting time,  $\gamma_{ac}$  is turned on for a time  $t_w$  during which we measure  $x_0$  and  $x_{90}$ . When performing several such experiments in the same nominal conditions, the relative dispersion observed is on the order of 25%.

(ii) the second protocol consists, as soon as the interface has been created, in applying to the slider a large amplitude harmonic shear force in order to make it slide a few micrometers in the direction of  $F_{dc}$ . The oscillating shear force is then suddenly stopped and a time  $t_w$  is waited, after which measurements are performed. The dispersion observed when using this second protocol is reduced to 11%. We will therefore present, in the rest of the paper, results that have been obtained on interfaces prepared this way.

This effect of the interface preparation on the reproducibility is illustrated on figure 3.

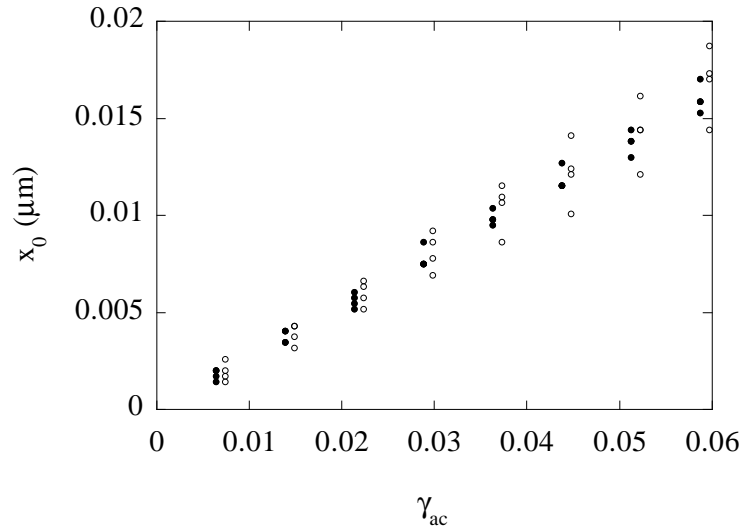


Figure 3. Influence of the protocol of interface preparation on the reproducibility. In-phase response  $x_0(\gamma_{ac})$  obtained with protocol (i) (○), and with protocol (ii) (●). Four sets of measurements are plotted, performed at  $f = 60$  Hz, with  $\gamma_{dc} = 0.27$  and after  $t_w = 300$  s.

To understand, at least qualitatively, the origin of this effect, note the following. When the slider is put into contact with the inclined track, the only mechanical condition which constrains the state of the MCI is that the total tangential force  $F = W \tan \theta$ . This is obviously insufficient to define uniquely the distribution of shear forces on the various microcontacts. Hence, a huge number of local configurations are possible: the interface is a highly multistable system. On the contrary, sliding produces a reproducible distribution which is maintained during the elastic recoil following a stop (Caroli & Nozières 1996, de Gennes 1997). Preparing an interface by interruption of sliding can therefore be expected to improve the degree of reproducibility. The remaining scattering of 11% is indeed in agreement with the statistical dispersion  $N^{-1/2} \approx 10\%$  due to the finite number of microcontacts estimated above.

### 3. Results

We present on figures 4 and 5 typical results obtained for the in-phase ( $x_0$ ) and out-of-phase ( $x_{90}$ ) components as a function of the reduced shear force amplitude  $\gamma_{ac}$ . We do not observe any dependence of the elastic or dissipative response on the level of average tangential force  $\gamma_{dc}$  (i.e. on the angle of inclination of the track, up to  $\gamma_{dc} \approx 0.36$ ), and do not note any frequency dependence in the explored range 15–100 Hz.

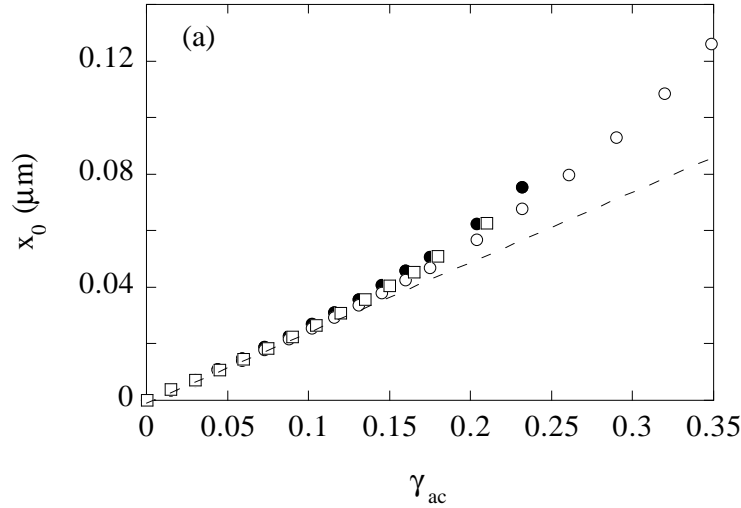


Figure 4. In-phase displacement amplitude  $x_0$  as a function of  $\gamma_{ac}$ , at  $f = 80$  Hz and after  $t_w = 600$  s. (□):  $\gamma_{dc} = 0$ , (○):  $\gamma_{dc} = 0.09$ , (●):  $\gamma_{dc} = 0.27$ .

Both  $x_0(\gamma_{ac})$  and  $x_{90}(\gamma_{ac})$  exhibit a linear regime at low shear amplitude, up to  $\gamma_{ac} \approx 0.1$  above which the interface responds non-linearly. For all the results presented in this article, in the range of  $\gamma_{ac}$  explored, no sliding is detected within the experimental resolution  $\approx 20$  nm.

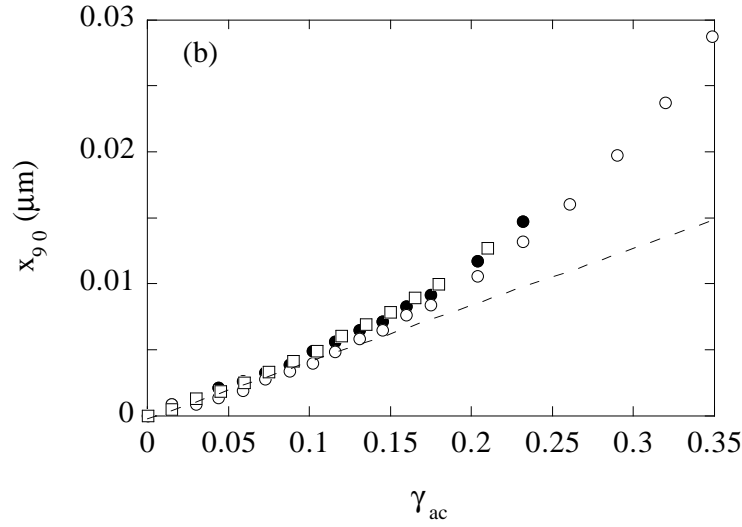


Figure 5. Out-of-phase displacement amplitude  $x_{90}$  as a function of  $\gamma_{ac}$ , at  $f = 80$  Hz and after  $t_w = 600$  s. ( ):  $d_c = 0$ , ( ):  $d_c = 0.09$ , ( ):  $d_c = 0.27$

(a) Linear response

In the linear regime, we measure the interfacial shear stiffness, which reads  $k_{ac} = \gamma_{ac} W / x_0$ . Moreover, we know that, for a multicontact interface, this stiffness varies proportionally to the normal load:  $k_{ac} = W / \ell$ , where  $\ell$  is an 'elastic length' which lies in the micrometer range (Berthoud & Baumberger 1998, see also section 4a for more details). The slope of  $x_0(\gamma_{ac})$  is thus  $\ell = dx_0/d\gamma_{ac}$ . We measure, after a waiting time  $t_w = 300$  s,  $\ell = 0.26 \pm 0.015$   $\mu\text{m}$ .

This length can also be determined by analyzing the frequency response of the system. Indeed, we expect that the response of the slider, of mass  $m$ , sitting on the elastic foundation of stiffness  $k_{ac}$  formed by the set of load-bearing asperities, exhibits a resonance at a circular frequency  $\omega_0 = \sqrt{k_{ac}/m} = \sqrt{g}$  (with  $W = mg$ ), as already observed by Sherif & Kossa (1991). When looking at the spectral response shown on figure 6, one clearly identifies a peak at  $f_0 = 1000$  Hz which corresponds to that resonance and leads to a value of the elastic length  $\ell = 0.25$   $\mu\text{m}$ , in excellent agreement with the value reported above.

Let us now try to identify the origin of the dissipation in this regime of very small shear amplitudes. We note that the inverse of the quality factor  $1/Q = 0.03$  of the resonance of figure 6 is comparable with the tangent of the loss angle  $\tan \delta = 0.05$  of bulk PMMA at 1 kHz and  $T = 300$  K (Ferry 1980). Besides, the ratio  $x_{90}/x_0 = 0.18$  is constant and on the order of  $\tan \delta = 0.1$  at  $f = 100$  Hz. This leads us to attribute the observed dissipation to the viscoelastic losses within the bodies of contacting asperities (more precisely, for each of them, within the volume of order roughly  $a^3$  (with  $a$  the mean contact radius) in which stresses concentrate. The discrepancy observed between  $x_{90}/x_0$  and the loss angle measured on bulk samples can be assigned to the fact that these micrometric volumes lie in the interfacial region, and hence most probably present mechanical properties slightly different

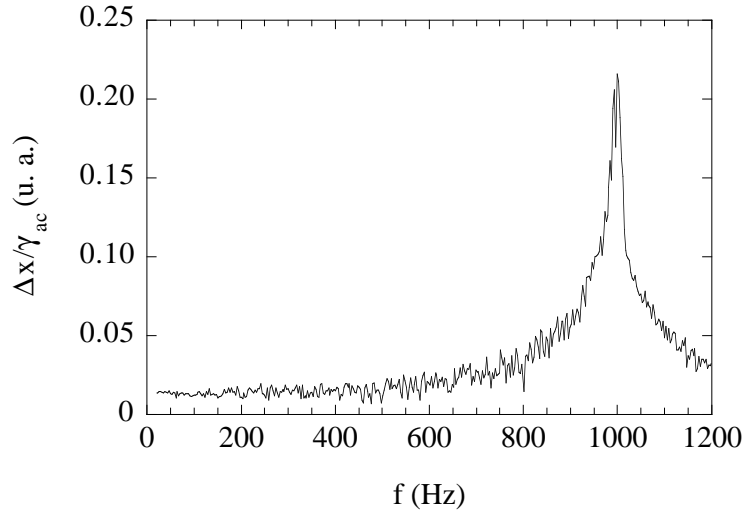


Figure 6. Spectral response: the slider is submitted to an acceleration of constant amplitude and variable frequency. The ratio of the displacement amplitude  $x$  to the acceleration amplitude is plotted, in arbitrary units, as a function of  $f$ . The bias  $\gamma_{dc} = 0$ .

from those of the bulk. Indeed, our method for surface abrasion (see x2a) makes use of water, known as a plasticizer of PMMA.

#### (b) Ageing

When performing measurements in the linear regime at various waiting times  $t_w$ , we note that the interfacial shear stiffness, or equivalently the elastic length  $\ell$ , evolves slowly with  $t_w$ : the longer  $t_w$ , the lower  $\ell$ , i.e. the higher the stiffness. This ageing of the interface is illustrated on figure 7. The elastic length decreases quasi-logarithmically with the age of the interface:

$$(\ell_w) = \ell_0 - \ln(t_w/t_0) \quad (3.1)$$

with the reference time  $t_0 = 1$  s,  $\ell_0 = 0.33$  and the logarithmic slope  $\beta = 1.07 \cdot 10^{-2}$ .

#### (c) Non-linear regime: interfacial dissipation

At shear amplitudes  $\gamma_{ac} > 0.1$ , the in-phase and out-of-phase components of the response increase non-linearly. In this regime, while the bulk response of the asperities remains linear (one can estimate a mean shear strain as the ratio of  $x_0$  to the mean contact size  $a$ , which stays lower than 2%), the ratio  $x_{90}/x_0$  is not constant anymore, hence the energy loss cannot be attributed to bulk viscoelasticity only.

We show on figure 8 the evolution, with shear amplitude, of the non-viscoelastic part of the dissipative response, which we define as  $x_{90} - x_0 \tan \delta$ , using for  $\tan \delta$  the value  $x_{90}/x_0 = 0.18$  determined in the linear regime.



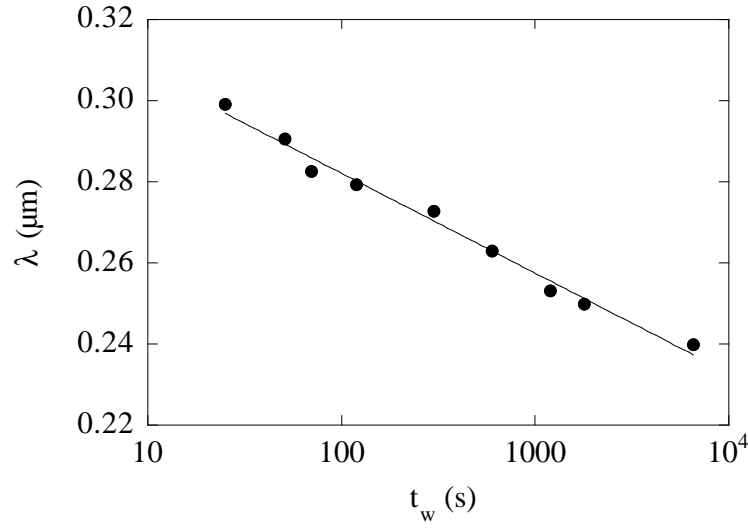


Figure 7. Decrease of the elastic length  $\lambda$  with the waiting time  $t_w$ .  $f = 80$  Hz,  $d_c = 0.18$ ,  $a_c = 0.04$ .

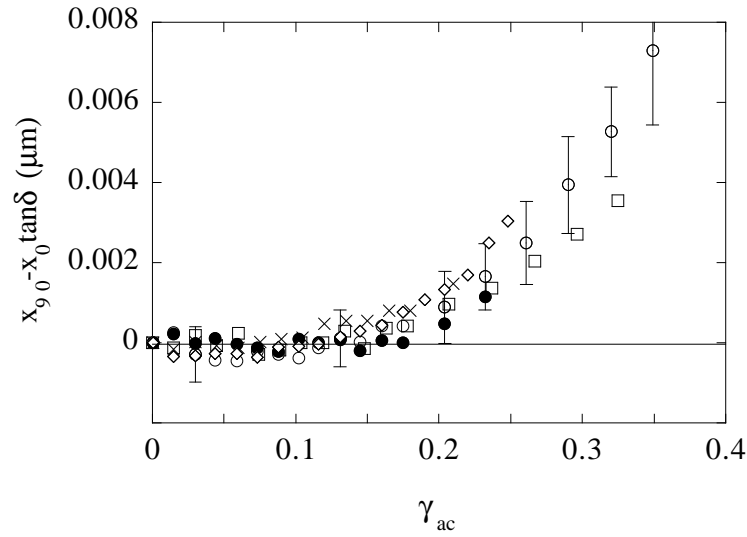


Figure 8. Non-viscoelastic component of the dissipative response,  $x_{90} - x_0 \tan \delta$ , as a function of  $\gamma_{ac}$ .  $f = 80$  Hz and  $t_w = 600$  s. ( ):  $d_c = 0$ , ( ):  $d_c = 0.09$ , ( ):  $d_c = 0.18$ , ( ):  $d_c = 0.27$ , ( ):  $d_c = 0.36$ .

#### 4. Discussion

##### (a) Interfacial shear stiffness

Let us consider the case of an infinitesimal shear modulation. In this limit, the shear stiffness of a single contact is simply given by the Mindlin expression

calculated in the absence of slip, namely  $G_a$ , with  $a$  the contact radius and  $G = 4G/(2 - \nu)$ , where  $\nu$  and  $G$  are respectively the Poisson ratio and shear modulus of the contacting materials (Mindlin 1949). The shear stiffness of the multicontact interface then reads (Berthoud & Baumberger 1998):

$$k_s = N G a \quad (4.1)$$

with  $N$  the number of microcontacts and  $a$  their mean radius (this result is rederived in the Appendix). An important feature of Greenwood's description of the contact between rough surfaces is that the number of microcontacts varies linearly with the normal load  $W$ , whereas their mean size is independent of  $W$ . So, the interfacial stiffness is proportional to the load, i.e.  $k_s = W/\lambda$ , with an elastic length reading:

$$\lambda = \frac{H P}{G} \frac{1}{s} \quad (4.2)$$

Using for the PMMA shear modulus its quasi-static value  $G \approx 1 \text{ GPa}$ , Berthoud & Baumberger found from equation 4.2 an elastic length  $\lambda \approx 1 \text{ }\mu\text{m}$ , in agreement with their quasi-static measurements of the stiffness during loading-unloading cycles.

Our results, however, lead to values of  $\lambda \approx 0.25 \text{ }\mu\text{m}$  much smaller than those previously reported. This marked difference may have two distinct origins:

First, we clearly see from our experiments that the linear regime of interfacial response corresponds to elastic displacements of the slider of at most 20 nm (see figure 4). Such a resolution could not be achieved in the previous quasi-static experiments, and the stiffness measured in that study was most probably underestimated, due to non-linear effects, which thus led to overestimated values of  $\lambda$ .

Moreover, note from expression 4.2 that the elastic length is inversely proportional to the shear modulus. We thus expect the elastic response of the multicontact interface to be governed, in our experiments, by the dynamic modulus at the excitation frequency, i.e.  $G^0 \approx 2 \text{ GPa}$  (see x2a).

With this latter value for the dynamic modulus, along with those for the hardness and the surface characteristics given in section 2a, we obtain  $\lambda \approx 0.39 \text{ }\mu\text{m}$ . The elastic length that we estimate from the elastic properties of PMMA at the excitation frequency is therefore in good agreement with our experimental results.

#### (b) Ageing

We now address the question of the time-dependence of the elastic length. It is well established, since the pioneer work of Bowden & Tabor (1950), that the real area of contact ( $A_r$ ) between rough surfaces is in general a very small fraction of the nominal area. The normal stresses on the load-bearing asperities are thus on the order of the yield stress of the contacting materials, which results in bulk plastic creep of these asperities. As a consequence, the real area of contact slowly increases with the 'age' of the interface, i.e. with the time of contact between asperities, as unambiguously evidenced by Dieterich & Kilgore (1994). From an extensive study of the mechanical properties of polymer glasses, Berthoud et al. (1999a) have shown

that creep of the load-bearing asperities results in a quasi-logarithmic growth of  $x_r$ :

$$x_r = x_{r0} [1 + m \ln(1 + \frac{t_w}{t_c})] \quad (4.3)$$

with  $m$  and  $t_c$  two material parameters that can be identified from bulk mechanical tests. For PMMA at room temperature,  $m \approx [0.04 \text{ } 0.05]$ , and a higher bound for the cut-off time is  $t_c < 5 \cdot 10^{-3}$  s.

From expression 4.1 of the shear stiffness  $G = N/G_a = W/x_r$ , and with the real area of contact  $x_r = N/a^2$ , we find that the elastic length reads:

$$l = \frac{W}{G \cdot N \cdot x_{r0} [1 + m \ln(1 + \frac{t_w}{t_c})]} \quad (4.4)$$

To first order in  $m$ , this expression reads:

$$l = \frac{W}{G \cdot N_0} [1 - \frac{m}{2} \ln(1 + \frac{t_w}{t_c})] \quad (4.5)$$

We thus expect the elastic length to decrease quasi-logarithmically with  $t_w$ , with a logarithmic slope of  $m \approx 2$ . Indeed, when fitting the data of figure 7 with an expression of the form  $l = l_0 [1 - \frac{m}{2} \ln(1 + \frac{t_w}{t_c})]$ , leaving  $l_0$  and  $t_c$  as free parameters, the best fit is obtained for  $l_0 = 0.024$  and  $t_c = 10^{-3}$  s, these values being in full agreement with the expected ones. The observed dependence of the interfacial shear stiffness on the waiting time  $t_w$  thus results from the creep ageing of the microcontacts.

It is interesting to note that up to now, this mechanism of interfacial ageing has always been characterized through the time-dependence of the static friction threshold (see Berthoud et al. 1999a, and references therein), which is a 'destructive' method in the sense that the set of load-bearing asperities is renewed by sliding when the measurement is performed. On the contrary, our low-amplitude oscillating shear experiments provide a way to probe accurately the slowly evolving viscoelastic response of a given set of microcontacts, without any macroscopic sliding at the interface.

#### (c) Non-linear elasticity and energy dissipation: extension of Mindlin's model

Figures 4 and 5 clearly show that, for  $\alpha_c \approx 0.1$ , the interfacial elastic response becomes non-linear, while no gross sliding is observable. In the same regime, a non-linear dissipative response develops on top of the linear term attributable to bulk viscoelasticity (figure 8). This contribution must therefore be considered as resulting from interfacial dissipation proper.

The decrease of the 'local' interfacial stiffness,  $d_{ac} = dx_0$ , with increasing shear amplitude may be interpreted qualitatively as follows. The diameters of the microcontacts which form the interface are statistically distributed about the average value  $a$ . A finite shear necessarily leads to destroying the smaller ones. The larger

The cut-off time  $t_c$  could not be determined accurately at room temperature, and was inferred from the velocity dependence of the friction force (Baumberger et al. 1999, Bureau 2002).

the shear amplitude, the smaller the number of microcontacts which are still able to sustain the stress, hence a decreasing stiffness.

In order to describe quantitatively this regime, we now extend Mindlin's description to the case of a multicontact interface as follows:

(i) The contact between the two rough surfaces is described *à la Greenwood*, with the assumption of an exponential distribution of summit heights, and of elastic deformation of asperities. We believe the latter assumption to be inessential: indeed, we saw in §2a that though contacting asperities are in an elastic-plastic state, the value of the plasticity index is of order unity, which suggests that the normal stress profile in microcontacts is still close to the Hertz profile (Johnson 1985).

(ii) Mindlin's results give, for a given microcontact, the expression of the tangential force associated with a remote shear displacement  $x$ . This displacement, equal to that of the center of mass of the slider, is common to all microcontacts.

(iii) For any finite  $x$ , there always exists a set of small microcontacts which are completely slipping. For these, the tangential force is saturated at its constant maximum value  $w$ , where  $w$  is the normal load on the microcontact.

(iv) The tangential force on the slider is simply the sum of those on the various microcontacts.

The detailed calculation is performed in the Appendix. It yields the following results:

$$x_0 = 2 \left[ \frac{ac}{2} + \frac{ac^2}{2} + \frac{5}{4} \frac{ac^3}{2} + O \left( \frac{ac^4}{2} \right) \right] \quad (4.6)$$

$$x_{90} = \frac{4}{3} \left[ 1 - \frac{2}{ac} \ln \left( 1 - \frac{ac}{2} \right) \right] = \frac{2}{3} \left[ \frac{ac^2}{2} + \frac{ac^3}{2} + O \left( \frac{ac^4}{2} \right) \right] \quad (4.7)$$

with the elastic length defined above. The local friction coefficient of Mindlin's model,  $\mu$ , is our single fitting parameter.

Figure 9 shows the best fit thus obtained for the elastic part of the response  $x_0$ , which is seen to be excellent. It corresponds to  $\mu = 0.49$ . On the other hand, from the response to a linear ramp of shear amplitude (see figure 1), we have estimated the ('global') static friction coefficient  $\mu_s$  as corresponding to a threshold of accelerated sliding. We thus find  $\mu_s = 0.59 \pm 0.03$  (Bureau et al. 2001). This can only be considered as a rough estimate, in view of the arbitrariness in the definition of the threshold. The agreement therefore appears quite satisfactory.

At this stage, we have determined all the parameters of the model, and are thus in a position to truly check its validity by comparing its prediction for  $x_{90}(ac)$  with the experimental results. The dissipation calculated from equation (4.7) with  $\mu = 0.49$  is plotted on figure 10: it is seen to be much larger than the experimental one. In order to get a decent fit of the data, we have to use a value of  $\mu$  as large as 1.3, i.e. much larger than any value of the friction coefficient ever reported for PMMA. The question therefore arises of what might be the physical reason for such a discrepancy which affects primarily the dissipative part of the response.

In Mindlin's model, dissipation results from the slip at the periphery of the contact. The inner radius of this annulus is, for an average microcontact,  $c =$

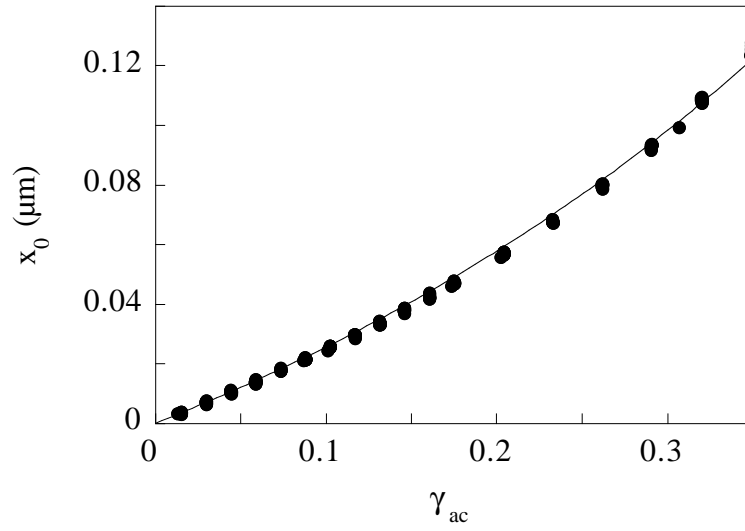


Figure 9. (•): experimental data for  $x_0(\gamma_{ac})$  at  $f = 80$  Hz and  $\nu_{dc} = 0.09$ . (—): extended Mindlin's model with  $\mu = 0.23$  m and  $\nu = 0.49$ .

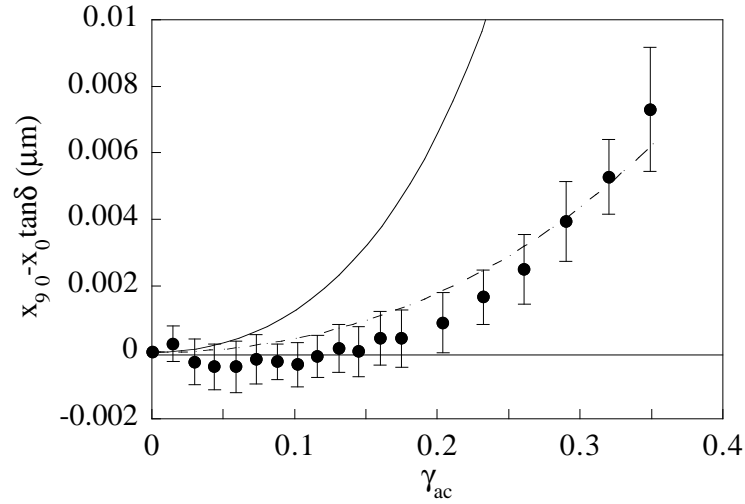


Figure 10. (•): experimental data for  $x_{90}(\gamma_{ac})$  at  $f = 80$  Hz and  $\nu_{dc} = 0.09$ . (—): extended Mindlin's model with  $\mu = 0.23$  m and  $\nu = 0.49$ . (---): extended Mindlin's model with  $\mu = 0.23$  m and  $\nu = 1.3$ .

a  $[f = (w/\lambda)^{1/3}]$ . For  $a = 5$  m and taking  $f = w = 0.2$  y we find, for  $\nu = 0.49$  that the width of the annulus  $a_{ac} = 750$  nm. Over this distance, the shear stress varies from its maximum value to zero at the edge of the contact. We have thus tacitly

used for the ratio  $f = w$  a typical value of the macroscopic ratio  $F = W$ . This amounts to assuming that  $N$  identical microcontacts of size  $a$  bear the same fraction of normal ( $w = W = N$ ) and tangential ( $f = F = N$ ) load.

assumed that the Coulomb law is valid on a spatial scale much smaller than this width.

It is now well documented that frictional dissipation results from the depinning of structural elements located within the adhesive junctions between load-bearing asperities. The typical size of these elements is found to be nanometric (Nakatani 2001, Baumberger et al. 1999, Bureau et al. 2002). The friction force, as it is usually defined, is an average over the dynamics of a large ensemble of such elements. So, a reasonably meaningful friction coefficient cannot be defined on a scale smaller than, say, a hundred nanometers. This must be understood as a cut-off length below which the Mindlin stress profile probably becomes inaccurate. The above estimate of  $\alpha_c$  therefore suggests that multicontact interfaces with micrometric roughness might be out of the range of quantitative applicability of Mindlin's model.

## Appendix A. Extension of Mindlin's model

### (a) Mindlin's results

We first recall the results derived by Mindlin for the contact of identical elastic spheres submitted to a tangential force (Mindlin et al. 1953, Johnson 1985). When the contact is first loaded from zero, the relationship between the remote tangential displacement  $x$  and the applied shear force  $f$  reads:

$$x = \frac{3(2-\nu)}{8Ga} w^{2/3} \left(1 - \frac{f}{f_m}\right)^{3/2} \quad (\text{A } 1)$$

with  $G$  the shear modulus,  $\nu$  the Poisson ratio,  $a$  the Hertz radius of contact,  $w$  the normal load and  $f_m$  the local friction coefficient.

If the shear force is then decreased, after having reached a maximum value  $f_{m \max}$ , the displacement  $x_{\text{un}}$  in this unloading phase is:

$$x_{\text{un}} = \frac{3(2-\nu)}{8Ga} w^{2/3} \left(1 - \frac{f_{m \max}}{f_m}\right)^{3/2} \left(1 - \frac{f}{f_{m \max}}\right)^{3/2} \quad (\text{A } 2)$$

By symmetry, if the shear force is then reversed from a value  $f_{m \max}$ , the displacement  $x_{\text{re}}(f) = -x_{\text{un}}(-f)$ .

### (b) Contact between rough surfaces

The contact geometry is that of two rough surfaces of identical rms roughness  $s$ . We shall consider, within the framework of Greenwood's model, the case of contact between a rigid, ideally smooth, reference plane and a composite rough surface whose summit heights are distributed exponentially:  $(z) = s^{-1} \exp(-z/s)$ , with  $s = \sqrt{2} \sigma$  (Berthoud & Baumberger 1998). The coordinate  $z$  is normal to the mean plane of the random surface.

The effective elastic modulus of the deformable material is defined as  $E^* = E/[2(1-\nu^2)]$ , and the equivalent radius of curvature at the tip of asperities for the composite surface is  $R^* = R/\sqrt{2}$ .

For a given normal load on the solids, we note  $h$  the distance between the mean plane of the rough surface and the reference flat. The compression of a contacting asperity of height  $z > h$  is thus  $\delta = z - h$  (Greenwood & Williamson 1966).

## (c) First loading of the multicontact interface

We now calculate the interface response when the shear displacement  $x$  first increases from 0 to  $x_{max}$ .

For each microcontact, the Hertz radius  $a$  and the normal load  $w$  depend on the compression  $z = z - h$ :

$$a = \sqrt[3]{\frac{P}{R(z-h)}} \quad (\text{A } 3)$$

$$w = \frac{4E}{3R} a^3 = \frac{2}{3} \frac{E}{(1-\nu^2)} \sqrt[3]{\frac{P}{R(z-h)^{3/2}}} \quad (\text{A } 4)$$

Plugging (A 3) and (A 4) into equation (A 1), and using  $G = E/(2(1+\nu))$ , we obtain:

$$1 - \frac{f}{w} \sqrt[2]{\frac{xs}{(z-h)}} = 1 - \frac{xs}{(z-h)} \quad (\text{A } 5)$$

where  $\nu = s(2-\nu) = [2(1-\nu)]$ .

We note that the rhs term of equation (A 5) is 0 for:

$$z - h = \frac{xs}{\sqrt[2]{\frac{xs}{(z-h)}}} \quad (\text{A } 6)$$

This means that microcontacts whose compression  $z - h$  satisfies condition (A 6) bear a tangential force  $f = w$ . Microcontacts such that  $z - h = xs = (\dots)$  are totally sliding, i.e.  $f = w$ .

In the following, we will assume that 'small' contacts such that  $z - h < xs = (\dots)$  are also sliding and bear a tangential force equal to  $w$ .

Hence, for microcontacts such that (A 6) is verified, equation (A 5) leads to:

$$\frac{f}{w} = \frac{2E}{3(1-\nu^2)} \sqrt[3]{\frac{P}{R(z-h)^{3/2}}} \left( 1 - \sqrt[2]{\frac{xs}{(z-h)}} \right) \sqrt[3]{\frac{xs}{(z-h)}} \quad (\text{A } 7)$$

The total tangential force on the system is obtained by integration over the height distribution:

$$\begin{aligned} \frac{F}{N_0} = & \frac{2E}{3(1-\nu^2)} \sqrt[3]{\frac{P}{R}} \left( \int_{h_0}^{Z+1} \frac{1}{(z-h)^{3/2}} \sqrt[2]{\frac{xs}{(z-h)}} \sqrt[3]{\frac{xs}{(z-h)}} dz \right. \\ & \left. + \int_h^{Z_{h_0}} \frac{1}{(z-h)^{3/2}} \sqrt[2]{\frac{xs}{(z-h)}} \sqrt[3]{\frac{xs}{(z-h)}} dz \right) \quad (\text{A } 8) \end{aligned}$$

where  $N_0$  is the total number of asperities, and  $h_0$  is given by condition (A 6). The first integral corresponds to the contribution of microcontacts whose response is given by (A 7), while the second term corresponds to totally sliding contacts.

Actually, when the interface is sheared, the smallest microcontacts are destroyed and replaced by new ones, the contribution of which we cannot calculate. We will see further that the interfacial response is not significantly affected by this assumption.

Setting  $z = (z - h) = s$ , and noting that the total normal load on the interface reads, according to Greenwood:

$$W = \frac{(4/3)E^* \frac{P}{R} N_0 s^{3/2} e^{-h/s}}{\int_0^{z+h} \frac{1}{z} dz} \quad (A 9)$$

we finally get the following expression for the macroscopic shear force:

$$F = W \left( 1 - e^{-\frac{x}{s}} \right) \quad (A 10)$$

Inverting (A 10) yields:

$$x = s \ln \left( 1 + \frac{F}{W} \right) \quad (A 11)$$

In the limit of small tangential displacements, to lowest order in  $x = s \ln \left( 1 + \frac{F}{W} \right)$ ,  $F = W x = \frac{W}{s} x$ . We thus find the expression of the interfacial shear stiffness  $k = \frac{dF}{dx} = \frac{W}{s}$ , where  $s = \frac{2}{3} \left( \frac{P}{R} \right)^{1/2} \left( \frac{4}{3} E^* \right)^{-1/2}$  is the elastic length. For numerical purposes, we will however not estimate  $s$  from this expression but will rather make use of its experimentally measured value  $s \approx 0.25 \text{ nm}$ .

Finally, evaluating, from equation (A 8), the relative contribution of totally sliding microcontacts, we find that they contribute less than 10% to the calculated shear force while the tangential displacement stays lower than 60 nm (which corresponds to reduced shear force amplitudes  $\alpha_c \approx 0.2$ , see e.g. figure 4). Their contribution is at most 20% for  $x \approx 100 \text{ nm}$ .

#### (d) Unloading from $(F_{max}; x_{max})$

Let us now study the case where the tangential displacement of the slider is decreased, after having reached a maximum value  $x_{max}$ , corresponding to a maximum shear force  $F_{max}$ . Two families of microcontacts must then be considered:

(i) Microcontacts such that  $(z - h) < x_{max} s = (x_c)$

At the end of the first loading, these microcontacts are totally sliding. For  $x = x_{max}$ , the shear force on one of them is  $f_{max} = \mu w$ , and its response when  $x$  is decreased is given by (Mindlin et al. 1953, Johnson 1985):

$$x_c = x_{max} - \frac{3 \left( \frac{2}{3} \right)^{1/2} \mu w}{4 G a} \left( 1 - \frac{b^2}{a^2} \right) \quad (A 12)$$

where  $b$  is the inner radius of the corresponding slip zone:  $b = a \left[ 1 - \frac{f}{\mu w} \right]^{1/3}$ . We thus obtain:

$$\frac{1}{2} + \frac{f}{2 \mu w} \left( \frac{x_{max}}{s} \right)^{2/3} = 1 - \frac{(x_{max} - x_c) s}{2 (z - h)} \quad (A 13)$$

y This estimate is done using  $\mu = 0.49$ , the value which leads to the best fit of  $x_0(\alpha_c)$  (see figure 9). A higher value of  $\mu$  would lead to an even weaker contribution of sliding contacts.



As in xc, this equation yields the following condition:

$$z - h = \frac{(x_{m \text{ ax}} - x_g)s}{2} \quad (\text{A } 14)$$

Microcontacts whose compression satisfies condition (A 14) respond according to equation (A 13), while those for which  $z - h < (x_{m \text{ ax}} - x_g)s/2$  are assumed to be totally sliding and bear a tangential force  $f = \mu w$ .

For the contacts which are not fully sliding during unloading, equation (A 13) yields:

$$\frac{f}{w} = \frac{2E}{3(1-\nu^2)} \frac{P}{R} \left( \frac{z - h - \frac{(x_{m \text{ ax}} - x_g)s}{2}}{(z - h)^{3/2}} \right)^{3/2} \quad (\text{A } 15)$$

(ii) Microcontacts such that  $(z - h) \geq \frac{(x_{m \text{ ax}} - x_g)s}{2}$

The response of these microcontacts, which were not totally sliding when  $x$  reached its maximum value, is given by (Mindlin et al. 1953, Johnson 1985):

$$x_g = \frac{3(2-\nu)}{8Ga} \frac{w}{2} \left( 1 - \frac{f_{m \text{ ax}}}{2w} \right)^{2/3} \left( 1 - \frac{f_{m \text{ ax}}}{w} \right)^{2/3} \quad (\text{A } 16)$$

From equation (A 5) we get:

$$1 - \frac{f_{m \text{ ax}}}{w} = 1 - \frac{x_{m \text{ ax}}s}{(z - h)} \quad (\text{A } 17)$$

which, once plugged into (A 16), leads to the following expression for the shear force on one of these microcontacts:

$$\frac{f}{w} = \frac{2E}{3(1-\nu^2)} \frac{P}{R} \left( \frac{z - h - \frac{(x_{m \text{ ax}} - x_g)s}{2}}{(z - h)^{3/2}} \right)^{3/2} \quad (\text{A } 18)$$

(iii) Total shear force

The macroscopic shear force when the interface is unloaded is the sum of the contributions (A 15), (A 18), and of that resulting from fully sliding microcontacts:

$$\begin{aligned} \frac{F}{W} = & \frac{1}{2} \left( \frac{z_{m \text{ ax}}}{z_0} \right)^{3/2} \left( 1 - \frac{x_{m \text{ ax}}}{2z_0} \right)^{3/2} \left( 1 - \frac{x_{m \text{ ax}}}{z_0} \right)^{3/2} e^{-d} \\ & + \frac{1}{2} \left( \frac{z_{m \text{ ax}}}{z_0} \right)^{3/2} \left( 1 - \frac{x_{m \text{ ax}}}{2z_0} \right)^{3/2} e^{-d} \\ & + \frac{1}{2} \left( \frac{z_{m \text{ ax}}}{z_0} \right)^{3/2} e^{-d}; \end{aligned} \quad (\text{A } 19)$$

which yields:

$$\frac{F}{W} = 2e^{\frac{x_{max} - x_0}{2}} e^{\frac{x_{max}}{2}} - 1 \quad (A 20)$$

Setting  $F=W$  yields:

$$x_0 = x_{max} + 2 \ln \left( 1 + \frac{x_{max}}{2} \right) \quad (A 21)$$

with  $x_{max}$  as given by (A 11):

$$x_{max} = \ln \left( 1 + \frac{x_{max}}{2} \right) \quad (A 22)$$

Finally, by symmetry, the relationship  $x(F)$  when the displacement, having reached a minimum value  $x_{min}$ , is reversed up to  $x_{max}$ , reads:

$$x_0 = x_{min} - 2 \ln \left( 1 + \frac{x_{min}}{2} \right) \quad (A 23)$$

with the minimum value of the displacement:

$$x_{min} = x_{max} + 2 \ln \left( 1 - \frac{x_{max}}{2} \right) \quad (A 24)$$

With a macroscopic shear force of the form  $F(t)=W \cdot (t) = x_{dc} + x_{ac} \cos(\omega t)$ , we obtain for the displacement response:

$$x_0 = \ln \left( 1 + \frac{x_{max}}{2} \right) + 2 \ln \left( 1 + \frac{x_{ac} (\cos(\omega t) + 1)}{2} \right) \quad (A 25)$$

and

$$x_0 = \ln \left( 1 - \frac{x_{max}}{2} \right) + 2 \ln \left( 1 - \frac{x_{ac}}{2} \right) - 2 \ln \left( 1 - \frac{x_{ac} (\cos(\omega t) + 1)}{2} \right) \quad (A 26)$$

#### (e) In-phase and out-of-phase components

The elastic and dissipative responses are given by:

$$x_0 = \frac{2}{T} \int_0^{\frac{T}{2}} x \cos(\omega t) dt = \frac{1}{T} \int_0^{\frac{T}{2}} x_0 \cos(\omega t) dt + \frac{1}{T} \int_0^{\frac{T}{2}} x_0 \cos(\omega t) dt \quad (A 27)$$

$$x_{90} = \frac{1}{T} \int_0^{\frac{T}{2}} x_0 \sin(\omega t) dt + \frac{1}{T} \int_0^{\frac{T}{2}} x_0 \sin(\omega t) dt \quad (A 28)$$

We expand in power of  $x_{ac} = (2) - 1$  the time-dependent logarithmic terms in equations (A 25) and (A 26), and finally get for the in-phase amplitude:

$$x_0 = 2 \left( \frac{x_{ac}}{2} + \frac{x_{ac}^2}{2} + \frac{5}{4} \frac{x_{ac}^3}{2} + O \left( \frac{x_{ac}^4}{2} \right) \right) \quad (A 29)$$

The out-of-phase component can be calculated exactly and reads:

$$x_{90} = \frac{4}{\pi} \left( 1 - \frac{2}{\pi} \ln \left( 1 + \frac{\pi}{2} \right) \right) \quad (\text{A } 30)$$

## References

- Baumberger, T., Bureau, L., Busson, M., Falcon, E. & Perrin, B. 1998 An inertial tribometer for measuring microslip dissipation at a solid-solid multicontact interface. *Rev. Sci. Instrum.* **69**, 2416{2420.
- Baumberger, T., Berthoud, P. & Caroli, C. 1999 Physical analysis of the state- and rate-dependent friction law: Dynamic friction. *Phys. Rev. B* **60**, 3928{3939.
- Berthoud, P. & Baumberger, T. 1998 Shear stiffness of a solid-solid multicontact interface. *Proc. R. Soc. Lond. A* **454**, 1615{1634.
- Berthoud, P., Baumberger, T., G'Sell, C. & Hiver, J.-M. 1999a Physical analysis of the state- and rate-dependent friction law: Static friction. *Phys. Rev. B* **59**, 14313{14327.
- Berthoud, P., G'Sell, C. & Hiver, J.-M. 1999b Elastic-plastic indentation creep of glassy poly(methyl methacrylate) and polystyrene: characterization using uniaxial compression and indentation tests. *J. Phys. D: Appl. Phys.* **32**, 2923{2932.
- Bowden, F. P. & Tabor, D. 1950 *The friction and lubrication of solids*. Oxford: Clarendon.
- Bureau, L., Baumberger, T. & Caroli, C. 2001 Jamming creep of a frictional interface. *Phys. Rev. E* **64**, 031502-1{031502-4.
- Bureau, L., Baumberger, T. & Caroli, C. 2002 Rheological aging and rejuvenation in solid friction contacts. *Eur. Phys. J. E* **8**, 331{337.
- Bureau, L. 2002 *Elasticité et rhéologie d'une interface macroscopique : du piégeage au frottement solide*. Ph.D. Thesis, Université Denis Diderot, Paris, France.
- Cattaneo, C. 1938 Sul contatto di due corpi elastici: distribuzione locale degli sforzi. *Rendiconti Accad. dei Lincei* **27**, pp 342{348, 434{436, 474{478.
- Caroli, C. & Nozières, Ph. 1996 . In *Physics of sliding friction* (ed. B. N. J. Persson & E. Tosatti), NATO ASI Series, series E: Applied Sciences, 311, Dordrecht: Kluwer.
- Courtney-Prat, J. S. & Eisner, E. 1956 The effect of tangential loading force on the contact of metallic bodies. *Proc. R. Soc. Lond. A* **238**, 529{550.
- Dietrich, J. & Kilgore, B. 1994 Direct observation of frictional contacts: new insights for state-dependent properties. *Pure Appl. Geophys.* **143**, 283{302.
- Ferry, J. D. 1980 *Viscoelastic properties of polymers*. New York: Wiley.
- de Gennes, P.-G. 1997 Friction force on a solid experiencing more than one contact. *C. R. Acad. Sci. Paris IIb* **325**, 7{14.
- Goodman, L. E. 1959 A review of progress in analysis of interfacial slip damping. In *Structural damping* (ed. J. E. Ruzicka), ASME annual meeting, pp 36{48.
- Goodman, L. E. & Brown, C. B. 1962 Energy dissipation in contact friction: constant normal load and cyclic tangential loading. *J. Appl. Mech.* **84** 17{22.
- Johnson, K. L. 1955 Surface interaction between elastically loaded bodies under tangential forces. *Proc. R. Soc. Lond. A* **230**, 531{549.
- Johnson, K. L. 1985 *Contact mechanics*. Cambridge: University Press.
- Mindlin, R. D., Mason, W. P., Osmer, T. F. & Deresiewicz, H. 1951 Effects of an oscillating force on the contact surfaces of elastic spheres. *Proc. of the 1st U.S. national congress of applied mechanics*, pp 203{208.
- Mindlin, R. D. 1949 Compliance of elastic bodies in contact. *J. Appl. Mech.* **71**, 259{268.
- Nakatani, M. 2001 Conceptual and physical clarification of rate and state friction: frictional sliding as a thermally activated rheology. *J. Geophys. Res.* **106**, 13347{13380.

- Olofsson, U. 1995 Cyclic micro-slip under unlubricated conditions. *Tribol. int.* 28, 207{217.
- Sherif H. A. & Kossa, S. S. 1991 Relationship between normal and tangential contact stiffness of nominally flat surfaces. *Wear* 151, 49{62.